Journal of Inclusion Phenomena and Macrocyclic Chemistry
https://doi.org/10.1007/s10847-026-01334-3

RESEARCH ARTICLE

Limits to the heterogenization of a copper-bispidine aziridination catalyst on NU-1000

Thomas Kieble[1] · Nadjana Schneider[1] · Tobias Saxl[2] · Frank Kirschhöfer[1] · Peter G. Weidler[1] · Stefan Heißler[1] · Thomas Josephy[2] · Katharina Bleher[1]

Received: 23 December 2025 / Accepted: 29 January 2026

Abstract
In this study, we investigated whether a tetradentate copper-bispidine complex can be heterogenized in the Zr-based metal-organic framework NU-1000. The ligand used is a rigid N-donor system based on the 3,7-diazabicyclo[3.3.1]nonane scaffold, and its copper complex is known for efficiently catalyzing the aziridination of styrene. Because different residual anions are commonly present in metal-organic frameworks, we first probed the influence of the counterion in homogeneous catalysis by synthesizing a series of copper-bispidine complexes bearing different counterions. In homogeneous solution under an inert atmosphere, the counterion had a pronounced effect on the aziridination yields. Under air, however, oxygen oxidized the catalytically active Cu(I) species, while water/hydroxido ligation became dominant and acted as co-ligands, thereby diminishing the impact of the counterion. Immobilization was targeted via solvent-assisted ligand incorporation (SALI). To this end, the methyl esters on the ligand backbone were converted to carboxylates to enable binding to the Zr_6O_6 nodes of NU-1000. Immobilization of the copper complex in NU-1000 follows Langmuir behavior; however, powder X-ray diffraction and attenuated total reflection - Fourier transform infrared spectroscopy measurements show that, under the conditions employed, the immobilization is predominantly superficial. Significant leaching prevented reliable catalytic testing of the immobilisates. Overall, direct SALI-based loading of the copper-bispidine system onto NU-1000 proved unstable; the results identify the key limitations (surface deposition and leaching) and suggest that alternative support materials or anchoring strategies may enable robust heterogenization of this catalyst class.

Keywords Metal–organic frameworks (MOFs)- NU-1000, Copper bispidine complexes, Solvent-assisted ligand incorporation (SALI), Aziridination catalysis

The authors Thomas Kieble and Katharina Bleher contributed equally to this work.

✉ Katharina Bleher
Katharina.bleher@kit.edu

Thomas Kieble
thomas.kieble@kit.edu

Nadjana Schneider
nadjana.schneider@student.kit.edu

Tobias Saxl
tobias.saxl@alumni.uni-heidelberg.de

Frank Kirschhöfer
frank.kirschhoefer@kit.edu

Peter G. Weidler
peter.weidler@partner.kit.edu

Stefan Heißler
stefan.heissler@kit.edu

Thomas Josephy
thomas.josephy@alumni.uni-heidelberg.de

[1] Karlsruher Institut für Technologie, Institut für Funktionelle Grenzflächen, Hermann-von-Helmholtz-Platz 1, Gebäude 330, D-76344 Eggenstein- Leopoldshafen, Germany

[2] Anorganisch-Chemisches Institut, Universität Heidelberg, INF 270, D-69120 Heidelberg, Germany

Published online: 17 March 2026

Introduction

The shift from homogeneous to heterogeneous catalysis is fundamental to sustainable process management and critical for eventual industrial use [1, 2]. Immobilization can reduce leaching of catalyst into products and enable catalyst reuse. In addition, confinement and anchoring on supports can mitigate aggregation or self-decay, extending catalyst lifetime. A broad toolbox now exists, especially for transition-metal complexes, spanning physisorption, ionic binding, covalent binding, pore encapsulation, and co-assembly e.g., linker integration in metal-organic frameworks (MOFs) [3, 4]. Supports range from porous inorganic frameworks (zeolites, MOFs) to polymer-based or magnetic beads, silica-based materials or hybrid materials [5–10]. In porous structures, catalysts can be immobilized by embedding them within the pores, where steric restrictions or attractive interactions ensure retention, or alternatively by tailored design of ligands or nanoparticles that form specific interactions with the metal nodes [11–16]. Alternatively, the ligand can be modified to also serve in building the MOF framework structure, thereby achieving covalent bonding. In this context, particularly for ruthenium- or palladium-based complexes, promising results have already been achieved, both in terms of immobilization and yields across various reactions [17–21]. Nevertheless, industrial deployment remains limited. In part, this reflects the high cost of immobilized catalysts, driven by the choice of support, as well as the fact that the expected advantages have not been reliably attained. For instance, numerous immobilized catalysts do not deliver sufficient stability or lag activity, resulting in metal leaching, diminished turnover numbers, and catalyst deactivation [22, 23].

Nevertheless, MOFs have proven particularly successful as supports for copper-catalyzed click reactions. Frequently used systems include HKUST-1, which is built from copper nodes, as well as zirconium-based MOFs that immobilize copper ions within the framework [24, 25]. Here, improved performance after immobilization of copper ions has often been observed [25, 26]. In these systems, high turnover numbers and good recyclability have been achieved, together with low leaching into the product. However, these are modifications that either exploit open metal sites in the MOF directly as catalytic centers or introduce additional ions to serve as catalysts. For the inclusion of transition-metal complexes, SALI (solvent-assisted ligand incorporation) has become the established method [27–29]: ligands are deliberately equipped with for example carboxylate groups in particularly for zirconium-based MOFs, so that they can coordinate to the Zr nodes of the framework. Popular ligand systems for this approach include porphyrins and pyridine-based motifs and it will now be investigated whether this strategy can be extended to the bispidine scaffold [30–34].

In the following, a bispidine framework will be modified so that it can be immobilized in a MOF via SALI. Bispidines are known for their rigid backbone and their highly tunable and adaptable synthesis [35]. The bispidine framework has already served as a modular scaffold for constructing coordination polymers. Cametti and co-workers showed that preorganized bispidine ligands support well-defined one-dimensional, often helical, coordination polymer architectures with metals such as Cu(II), Zn(II), and Hg(II), exhibiting guest-exchange dynamics and tunable porosity [36, 37]. The copper-bispidine complex used in this work is known to exhibit high turnover numbers in the homogeneous copper-catalyzed aziridination of styrene [38, 39], but it also suffers from the classical drawbacks of homogeneous catalysts, i.e. separation of the catalyst from the product by filtration through an absorbent material and thus loss of the catalyst. To overcome these drawbacks, this work investigates its immobilization via SALI within the zirconium-based MOF NU-1000 [40, 41]. This support material was specifically chosen as it is characterized by outstanding thermal and chemical stability, as well as a hierarchical pore structure. The large mesopores of NU-1000 (approx. 3.1 nm) are ideally dimensioned to accommodate the copper-bispidine complex, while simultaneously allow free access for substrates such as styrene [42, 43].

Materials and methods

All chemicals and reagents were purchased from ABCR, ACROS, Sigma-Aldrich or TCI and were used without further purification. Deuterated solvents for NMR spectroscopy were purchased from Deutero. Catalyses under Ar atmosphere were carried out in a glovebox Labmaster 130 (1250/780) from MBraun. Ligand L^1 [44], as well as Piperidone P^1 [45] (dimethyl 4-oxo-2,6-di(pyridin-2-yl)piperidine-3,5-dicarboxylate) and the oxidizing agent PhINTs were prepared as described before [46–48]. NU-1000 was purchased from CD bioparticles. Spectra were processed with Origin 2021b.

Mass Spectrometry (MS) experiments were carried out on an ApexQe hybrid 9.4 T FT-ICR (Fourier Transform - Ion Cyclotron Resonance) from Bruker. The measurements were carried out by the Mass Spectrometry Facility at the Department of Chemistry of Heidelberg University.

Elemental analyses (EA) were performed on a CHN-O Vario EL by the staff of the Department of Chemistry at Heidelberg University.

UV/vis−NIR spectra were recorded on an Agilent 8453 spectrophotometer equipped with an *USP-203-A* cryostat

from Unisoku or a Genesys 180 spectrometer from Thermo Scientific in UV-transparent 2.5 mL macro cuvettes. A Tecan spark plate reader with Greiner UV-STAR 96 well plates were used to determine the loadings of NU-1000.

Scanning Electron Microscopy (SEM) measurements with Energy Dispersive X-ray Spectroscopy were carried out on a Tescan VEGA3.

Inductively Coupled Plasma - Optical Emission Spectroscopy (ICP-OES) measurements were carried out on an Optima 8300DV from Perkin Elmer. Samples were digested in HCl/HNO_3 prior to analysis.

Attenuated Total Reflection - Fourier Transform Infrared Spectroscopy (ATR-FTIR) measurements were carried out using a Bruker Optics Tensor 27 spectrometer with room temperature deuterated triglycinesulfate (RT-DTGS) detector and a Bruker Optics Platinum® ATR accessory (diamond crystal with one reflection) has been applied (Bruker Optics, Ettlingen, Germany). All spectra were recorded at room temperature using the software Bruker OPUS 7.8.

Electrochemical measurements were performed on a 660D Electrochemical Workstation from CH Instruments with a three-electrode setup consisting of a glassy carbon working electrode (PFCE 3), a Pt wire counter electrode, and an $Ag/AgNO_3$ reference electrode (0.01 M Ag^+, 0.1 M $(Bu_4N)^+(PF_6)^-$ in MeCN) for organic solvents and an Ag/AgCl reference electrode (3 M NaCl in H_2O) for water. The solutions were purged with Ar and measurements were carried out under Ar atmosphere. Potentials are reported with respect to fc/fc^+ for organic solvents and with respect to $[Fe(CN)_6]^{3-/4-}$ for water.

X-ray crystallography was performed on a Bruker D8 Venture diffractometer (see SI for details). Plots of the crystal structures were created using Olex2 [49]. Crystallographic data for the structures reported have been deposited with the Cambridge Crystallographic Data Centre with the deposition numbers 2513653 (for $[(L^1)Cu^{II}(SO_4)]$), 2513655 (for $[(L^1)Cu^{II}(OAc)](OAc)$, 2513652 (for $([(L^1)Cu^{II}(NO_3)](NO_3)$), 2513654 (for $[(L^1)Cu^{II}(MeCN)](ClO_4)_2$), 2513651 (for L^2) and 2513650 (for $[(L^2)Cu^{II}(L^2)](OTf)$). The anion structure of $[(L^1)Cu^{II}(MeCN)](ClO_4)_2$ is severely disordered and treated with split positions. This results in a high R_{int}, and therefore the overall structure should be interpreted with caution.

Nuclear Magnetic Resonance (NMR) spectra were recorded at 200 MHz (^1H) on an Avance I or at 600 MHz (^1H) and 151 MHz (^{13}C) on an Avance III instrument from Bruker with the solvent as internal reference.

Powder X-Ray Diffraction (PXRD) measurements were carried out on a Bruker D8 A25 diffractometer equipped with a position-sensitive detector (PSD) Lynxeye in θ-θ geometry, variable divergence slit, an automatic knife-edge, and 2.3° Soller-slit on both sides. The PXRD data was acquired over a 2θ range of 1.5– 41.5° 2θ, with 1 s per 0.011° 2θ-step. The sample was rotated with 10 rounds per minute. Data assessment was carried out using Bruker's EVA 15.0 evaluation program and determination of cell parameters [50] and occupancies of Cu by TOPAS V6 [51].

High Performance Liquid Chromatography (HPLC) measurements for determination of the yield of the aziridination reaction were performed on a Hitachi HPLC Chromaster with a diode array detector. A Phenomenex® Gemini 3u C18 column was used and kept at 35 °C for analysis. The total flow rate was 0.6 mL/min, with an applied $MeCN/H_2O$ gradient. The injection volume was 10 µL. The absorbance measurement of styrene was performed at λ = 210 nm, and for 2-phenyl-1-tosylaziridine at λ = 227 nm (internal reference value 380 nm).

Standard procedures

More detailed procedures are given in the SI.

Direct immobilization in NU-1000

Two aqueous stock solutions of $[(L^2)Cu^{II}(H_2O)]^{2+}$ (24.61 mM and 9.66 mM) were acidified to pH 2 with concentrated HCl and sonicated until the complex was completely dissolved. Aliquots of these stocks and H_2O (pH 2) were added to pre-weighed NU-1000 to obtain the desired initial complex concentrations (see SI Table S 3). Suspensions were shaken at 65 °C for 24 h. After centrifugation supernatants were analyzed by UV/vis spectroscopy at 256 nm (Tecan Spark). The solids were washed twice with 1.000 mL ultrapure H_2O and dried under vacuum.

Stability test

To assess the stability under aziridination-like conditions, NU-1000 immobilisates were incubated with 1.000 mL acetonitrile at 25 °C for 24 h in a thermoshaker. The copper concentration in the supernatant was determined by ICP-OES. Four washing cycles were performed for each immobilisate.

Aziridination reactions

Homogeneous catalyses under argon were performed in a glove box using a 1.5 ml vial charged with 20 eq PhINTs (10 to 25 mg) and 100 eq styrene (10 to 40 µl). The reaction was started by adding a 5 mM solution of the copper complex (1 eq), dissolved in dry, absolute acetonitrile. The reaction duration was obtained through the poor solubility of the oxidant in MeCN, the moment the solution becomes clear is equal to the end of the reaction. For the determination of the catalytic yields, the reactions were stirred for 18 to 24

h in total, but at least until a clear solution was obtained. After removal from the glovebox, the mixture was filtered through a short silica pipette column, washed with ethyl acetate, and the filtrate was concentrated under reduced pressure. Yields were determined by ^{1}H NMR spectroscopy with 1,3,5-trimethoxybenzene (8 to 20 mg – exact amount was noted) as internal standard [39]. All experiments were performed twice (if a deviation of max 5% was obtained, else the experiments were repeated a third time).

Homogeneous catalyses under air were performed analogously to the argon experiments, but in 1.5 mL reaction tubes on a thermoshaker (≥18 h, 750 rpm, 25 °C). Owing to oxygen-induced side reactions, mixtures did not fully clarify; suspensions were therefore centrifuged, and the supernatants were diluted (1:100 – 1:1000 in MeCN/H_2O) for HPLC analysis. All experiments were performed in triplicate.

Syntheses

L^2: The synthesis of L^2 was adapted from previously reported syntheses [39]. A detailed synthesis procedure and the characterization are provided in the SI (Figure S 1 – S 2).

General synthesis of the copper(II) complexes. The corresponding ligand and an equimolar amount of the used copper(II) salt were dissolved in MeCN or MeOH to obtain an intense blue 0.5 to 2 mM solution. The mixture was stirred for 30 min at rt for complete complexation. The complexes were obtained by ether diffusion as blue crystals in almost quantitative yields (90 to 98%).

$[(L^1)Cu^{II}(MeCN)](ClO_4)_2$. EA ($C_{22}H_{24}CuCl_2N_4O_{13}$ × H_2O) [%], calc: C, 37.49; H, 3.74; N, 7.95; found: C, 37.36; H, 3.94; N, 8.18. ESI-MS (pos., MeCN) *m/z*: 586.0526 (100%) $[(L^1)Cu^{II} + ClO_4]^+$ (calc: 586.0522).

$[(L^1)Cu^{II}(NO_3)](NO_3)$. EA ($C_{22}H_{24}CuN_6O_{11} \times 0.5\ H_2O$) [%], calc: C, 42.55; H, 4.06; N, 13.53; found: C, 42.70; H, 4.28; N, 13.48. ESI-MS (pos., MeCN) *m/z*: 522.0729 (100%) $[(L^1)Cu^{II} + Cl]^+$ (calc: 522.0731), 540.0836 (32%) $[(L^1)Cu^{II} + Cl + H_2O]^+$ (calc: 540.0837). *m/z*: 549.0921 (3%) $[(L^1)Cu^{II} + NO_3]^+$ (calc: 549.0915), 567.1026 (0.4%) $[(L^1)Cu^{II} + NO_3 + H_2O]^+$ (calc: 567.1027).

$[(L^1)Cu^{II}(Cl)](Cl)$. EA ($C_{22}H_{24}CuCl_2N_4O_5 \times 2\ H_2O$) [%], calc: C, 44.42; H, 4.74; N, 9.42; found: C, 43.87; H, 4.50; N, 9.57. ESI-MS (pos., MeCN) *m/z*: 522.0729 (55%) $[(L^1)Cu^{II} + Cl]^+$ (calc: 522.0731), 540.0836 (100%) $[(L^1)Cu^{II} + Cl + H_2O]^+$ (calc: 540.0837).

$[[(L^1)Cu^{II}(OAc)](OAc)$. EA ($C_{26}H_{30}CuN_4O_9 \times 3\ H_2O$) [%], calc: C, 47.31; H, 5.50; N, 8.49; found: C, 47.25; H, 5.44; N, 8.50. ESI-MS (pos., MeCN) *m/z*: 546.1174 (100%) $[(L^1)Cu^{II} + OAc]^+$ (calc: 546.1170).

$[[(L^1)Cu^{II}(SO_4)]$. EA ($C_{22}H_{24}CuN_4O_8S \times$MeCN x 2 H_2O) [%], calc: C, 43.60; H, 4.73; N, 10.59; found: C43.39; H, 4.61; N, 10.06. ESI-MS (pos., MeOH) *m/z*: 536.1333 (100%) $[(L^1)Cu^{II} + OH + MeOH]^+$ (calc: 536.1327), 624.0569 (12%) $[(L^1)Cu^{II} + SO_4 + H_2O + Na]^+$ (calc: 624.0563).

$[[(L^2)Cu^{II}(MeOH)](OTf)_2$. EA ($C_{27}H_{37}CuF_6N_5O_{14}S_2 \times 3$ MeOH) [%], calc: C, 36.14; H, 4.16; N, 7.81; found: C, 36.63; H, 4.35; N, 8.13. ESI-MS (pos., MeOH) *m/z*: 550.1486 (79%) $[(L^2)Cu^{II} + OMe + H_2O]^+$ (calc: 550.1483), 668.0824 (100%) $[(L^2)Cu^{II} + OTf + H_2O]^+$ (calc: 668.0820).

Results

The copper bispidine complex L^1 (see Fig. 1) is characterized by its high yield and turnover frequency in the homogeneous aziridination of styrene. To develop a heterogeneous version of this catalyst, SALI will be employed to attach the copper complex to the Zr_6O_6 nodes in NU-1000. To enable anchoring, the methyl ester groups on the bispidine backbone need to be hydrolyzed to the corresponding carboxylic acids, thereby providing the necessary functionality for coordination to the zirconium nodes. For this purpose, L^2 was synthesized based on a literature-known synthesis [39]. Briefly, ligand L^1 was first treated with $NaBH_4$ overnight to reduce the ketone at C^9 of the backbone to the corresponding alcohol (see Fig. 2). This prevents retro-Mannich reaction and makes the backbone robust against extreme pH values, needed for saponification in the following reaction step as well as in later immobilization steps on the support material. Subsequently, the methyl esters of the side groups were saponified with NaOH to obtain the desired carboxylic acids for binding to the zirconium nodes. L^2 was obtained with a yield of 65%.

The ligand was then complexed with $Cu(OTf)_2$ to afford the copper complex. Crystals suitable for single-crystal X-ray diffraction were obtained for both the free ligand and the copper complex from MeOH/water over several months. The crystal structure of the complex is shown in Fig. 3. Intermolecular coordination of the ligand's carboxylate groups to a neighboring copper center is observed. This behavior may have been promoted by the prolonged crystallization period and repeated solvent exchange to induce crystal growth. However, a similar motif is also observed for the ligand, where the carboxylate groups coordinate to sodium cations (SI Figure S 3). Both ligand and complex exhibit a pronounced tendency to form chain-like assemblies, which strongly affects their solubility, particularly in organic solvents.

In addition to the triflate complex, a series of $[(L^1)Cu^{II}(X)]^{n+}$ complexes was prepared with different counterions (OAc^-, SO_4^{2-}, NO_3^-, ClO_4^- and Cl^-). MOFs often retain salts from synthesis, take up additional ions during immobilization, or require specific buffers for immobilization

protocols. However, it is known that counterions influence copper-catalyzed aziridination [47, 52]. This series was therefore designed to probe the influence of counterions on the aziridination reaction. Single crystals suitable for X-ray analysis could be obtained by ether diffusion from MeCN or MeOH. The key structural parameters of the synthesized complexes are summarized in Table 1 (full crystallographic data and structures are provided in the SI). All crystal structures show the expected pseudo tetragonal geometry. The structural data show that coordinating counterions indeed affect the complex geometry. In particular, the elongated axis of the complex changes. While in the presence of coordinated acetonitrile the N3-Cu-X axis is elongated (for OTf^- and ClO_4^-), complexes with coordinating counterions show elongation of the N7-Cu axis, i.e., along the position that does not bear the negative charge of the counterion (in $[(L^2)Cu^{II}(L^2)]^+$, the counterion is a deprotonated ligand L^2). This behavior is consistent with the expected pseudo Jahn-Teller-type distortion of Cu(II) centers, which is redistributed depending on the donor strength and position of the respected counterion or co-ligand.

After the solid-state structures of the complexes had been examined, the structures of the complexes in solution were investigated. All measured values are listed in Table 2 and spectra are shown in the SI Figures S 10 - S 12. Bispidine-Cu(II) complexes have an unpaired electron in the d_{x2-y2} orbital and show a d-d transition from the dπ orbitals at around 620 – 650 nm in MeCN [39]. This transition was likewise observed for the complexes with triflate, nitrate, and perchlorate counterions. The UV/vis-NIR spectra of all other complexes could not be examined in MeCN due to their low solubility. From published $Cu^{II/I}$ studies with bispidine complexes, it is known that the complexes in solution have structures that are very similar to those in crystals, with one difference: a solvent molecule replaces the co-ligand in the solid state [54, 55]. In MeCN, however, this seems to apply only to the weaker coordinating counterions, while the stronger coordinating counterions contribute to the insolubility of the complexes. Therefore, the complexes were remeasured in MeOH. Here, too, a band around 600 – 650 nm is visible, as well as a shoulder at around 700 nm in some of the spectra. In MeOH, the ligand field is slightly altered compared to MeCN, either due to effects of the secondary coordination sphere or to the coordination of methanol, methanolate, or water. Since Cu(II) complexes with an elongated octahedral or square-pyramidal geometry exhibit more than one formally spin-allowed but Laporte-forbidden d-d transition, this change in ligand field leads to a clearer separation of these transitions. As a result, in MeOH a second band appears at lower energy (ca. 700 nm) in addition to the main band around 600 – 652 nm, reflecting the modified splitting pattern of the d orbitals under these conditions [56, 57]. The complex $[(L^2)Cu^{II}(H_2O)]^{2+}$ dissolves only poorly in MeOH and MeCN due to its carboxylic acid groups; measurements were therefore carried out in water. As with the MeOH measurements on the other complexes, the UV/vis-NIR spectrum shows a broad band around 600 nm with a shoulder. This likewise suggests coordination of a solvent-derived ligand at the copper center, i.e., H_2O/HO^- in water (and $MeOH/MeO^-$ in MeOH) or changes in the secondary coordination sphere.

In addition to the UV/vis-NIR data, the redox potentials of the complexes were determined (see SI Figures S 6 - S 9). This parameter is expected to play an important role in aziridination, alongside reversible deprotonation (in the present system), and steric effects [58]. Where possible, the redox potentials were measured in both MeCN and MeOH. The complex with L^1 is known to exhibit a relatively positive redox potential of approximately −400 mV vs. fc/fc^+ in MeCN compared to other tetradentate bispidine complexes, which show potentials around − 500 mV in MeCN [39]. The measurements in MeCN clearly differentiate cases in which the solvent is coordinated from those in which a negatively charged counterion is bound, the latter leading to a shift toward more negative potentials. In MeOH, the potentials are comparatively similar, consistent with OH^-/MeO^- coordination in cases where the counterion is not coordinated, as also indicated by the UV/vis-NIR data.

Homogeneous aziridination of styrene

In addition to the characterization of the copper complexes, the catalytic performance of the complexes with L^1 bearing different counterions, as well as the complex with L^2, was evaluated in the homogeneous aziridination of styrene. The reactions were carried out both under argon and under air. Catalytic aziridination proceeds via an active Cu(I) species, so that part of the PhINTs ((N-(p-toluenesulfonyl)imino) phenyliodinane) added to the reaction is required to reduce Cu(II) to Cu(I) to generate the catalytically active species (see Fig. 4). Under air, molecular oxygen can reoxidize the active Cu(I) species to catalytically inactive Cu(II), leading to additional, unproductive consumption of PhINTs. Consequently, a lower aziridination yield is expected under air compared to reactions carried out under inert gas [59]. The results of the catalytic experiments are summarized in Table 3.

The results under argon show yields between 57% and 68%, with two notable outliers. $[(L^1)Cu^{II}(MeCN)](OTf)_2$ gives the highest yield (82%), while $[(L^1)Cu^{II}(Cl)]Cl$ shows the lowest yield (37%). This deviation in yield can be attributed to the counterions used as described by Rodriguez et al., who have shown that halides can influence the reaction mechanism of copper-catalyzed aziridinations. When a

halide is coordinated to the copper center, the rate-determining step shifts from the formation of the copper-nitrene species to the formation of the C-N bond (see Fig. 4 for reaction mechanism) [60]. Furthermore, Evans et al., among others, observed similarly reduced yields when using halide counterions (Cl^-, Br^-) compared to other counterions, which is consistent with the adverse effect of halide coordination in copper-catalyzed aziridination reactions [47, 60, 61]. In our experiments, complexes bearing more weakly coordinating counterions tend to give slightly higher yields than those with more strongly coordinating anions [62–64]. However, with the exception of chloride and triflate, it is difficult to assess whether the observed differences in yield reflect a change in the rate-limiting step of the catalytic cycle, or whether the more strongly coordinating counterions primarily impede formation of the nitrene species by hindering dissociation of the co-ligand (the counterion) [46, 65]. In addition, some of the complexes are poorly soluble in MeCN and initially exist as a heterogeneous phase, only dissolving completely over the course of the reaction. This is expected to primarily affect the initial reaction rate and, under the chosen reaction times, should have only a minor influence on the endpoint catalytic yield. However, at longer reaction times a decrease in yield may nonetheless be expected, as the contribution of competing side reactions typically increases [46, 62, 65]. Under air, the results are more uniform: the yield observed is around 50% with respect to the amount of oxidant used, for all complexes except $[(L^2)Cu^{II}(MeCN)](OTf)_2$. This can be attributed to two effects. First, the samples are exposed to oxygen, which can remove the active Cu(I) species from the catalytic cycle through reoxidation, as described before, thereby reducing the potential yield. Second, working without inert gas allows water to penetrate the samples, which can lead to the formation of aqua or hydroxy complexes. This is supported by the spectroscopic and electrochemical characterization, and reduces the influence of the counterions, leading to more uniform behavior. The drastic drop in yield for $[(L^2)Cu^{II}(MeCN)](OTf)_2$ can be explained as follows: as mentioned above, the complex is poorly soluble in MeCN, the solvent used for the catalytic reactions. Consequently, the catalyst concentration at the start of the reaction is very low and only increases slowly over the course of the reaction.This is expected to slow the reaction rate substantially, so that the effect of atmospheric oxygen is even more pronounced than in the other experiments conducted in air. In general, the reactions remain feasible under air despite the decrease in yield caused by O_2. These experiments were small batch tests with high O_2 supply (low reaction volume, large gas-liquid interface). With the planned heterogenization, the influence of oxygen is expected to decrease as on the one hand, the reaction volume increases (lower surface-to-volume ratio), and on the other hand, the access of O_2 to the active center is partially restricted by diffusion into the support material (pores, boundary layers). In a possible subsequent continuous operation, a lower O_2 entry is also typically expected, further reducing its adverse effect. Therefore, the immobilization experiments described below are carried out under air.

Immobilization of $[(L^2)Cu^{II}(H_2O)]^{2+}$ in NU-1000

To enable transfer of the catalyst $[(L^2)Cu^{II}(H_2O)]^{2+}$ into an immobilized form, it was anchored on NU-1000. The immobilization strategy follows SALI as described in [27–29, 66]. This exploits the terminal zirconium sites in the NU-1000 metal nodes as well as the carboxylic acid groups of L^2 (see Fig. 1).

First, a two-step immobilization strategy was pursued, in which the ligand was immobilized on the NU-1000 support prior to complexation with Cu^{II}. In this approach, ligand uptake did not follow Langmuir-type saturation behavior but increased continuously with rising ligand concentration, implying that a multi-layer surface loading of NU-1000 takes place (see SI Figures S 19 and S 20). SEM images (see SI Figures S 22 - S 24) corroborated this. The characteristic rod-shaped NU-1000 crystals appeared agglomerated after incubation with the ligand, suggesting that the ligand forms the chain-like aggregates already observed in the crystal structures and thereby blocks the MOF pores.

Therefore, direct immobilization of the preformed copper complex was pursued in a second attempt. As shown in Fig. 5, the loading of the complex on NU-1000 follows Langmuir-type behavior (note: adsorption isotherms were recorded as single measurements due to limited material availability). For direct immobilization, NU-1000 was incubated with $[(L^2)Cu^{II}(H_2O)]^{2+}$ in water at pH 2, adjusted with concentrated HCl, at 65 °C for 24 h. The acidic conditions were chosen because of the poor solubility of the complex and to facilitate the displacement of residual species already residing in the pores of NU-1000 at the zirconium nodes. Also, concentrations higher than 15 mM could not be used, as the solubility of the complex became limiting. To contextualize the loading, the theoretical monomolecular loading of NU-1000 can be calculated: Immobilization of $[(L)Cu^{II}(H_2O)]^{2+}$ targets coordination of the deprotonated carboxylate groups to the zirconium cations of the framework [27]. Since some zirconium centers in the NU-1000 nodes are shielded by internal linker connectivity, at most four potential docking sites per node are available for binding of the carboxylate groups. This leads to a theoretical maximum loading $q_{max,\ theo}$ of 1.84 µmol/mg. The theoretical maximum is clearly higher than the monomolecular loading obtained from the Langmuir isotherm in Fig. 5 of q_{max} = 0.82 µmol/mg. This corresponds to 45%. This is realistic,

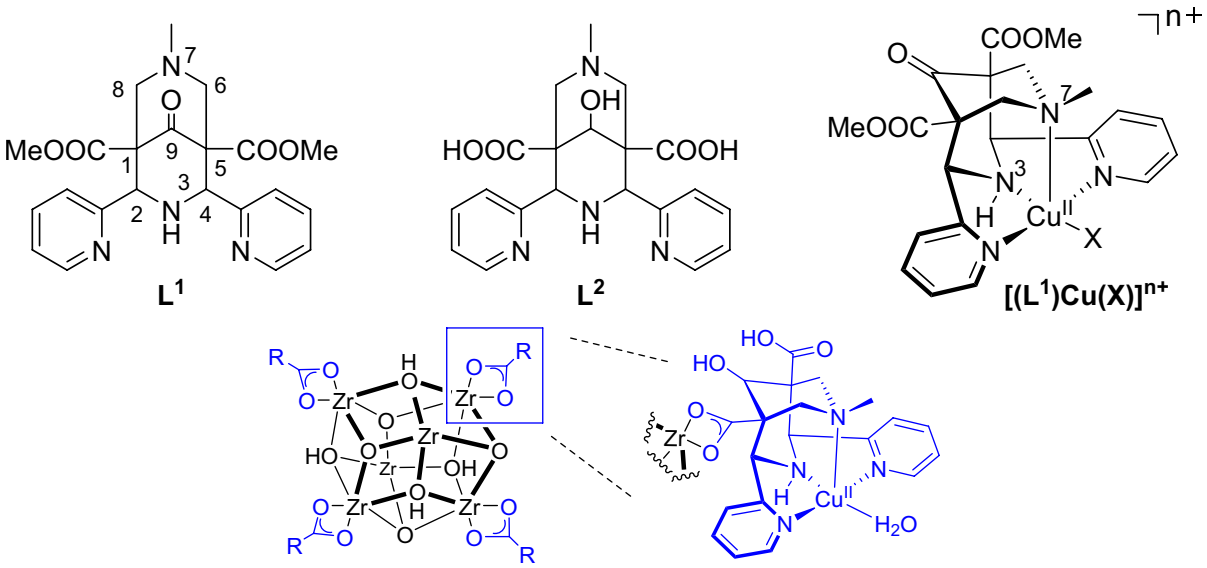

Fig. 1 Top: Used ligands in this manuscript. The atom numbering is shown in L^1. The complex geometry is also shown with L^1, where X is either a solvent molecule or a counterion. Bottom: Substitution of endcapping groups of a Zr_6O_6 node (e.g. formate) with carboxyl groups of $[(L^2)Cu^{II}(H_2O)]^{2+}$

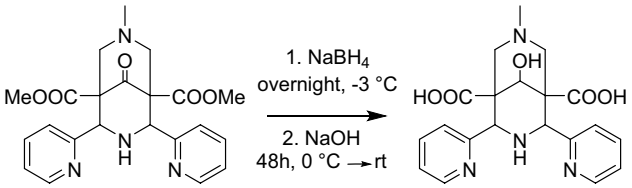

Fig. 2 Synthesis of the Ligand L^2 starting from L^1

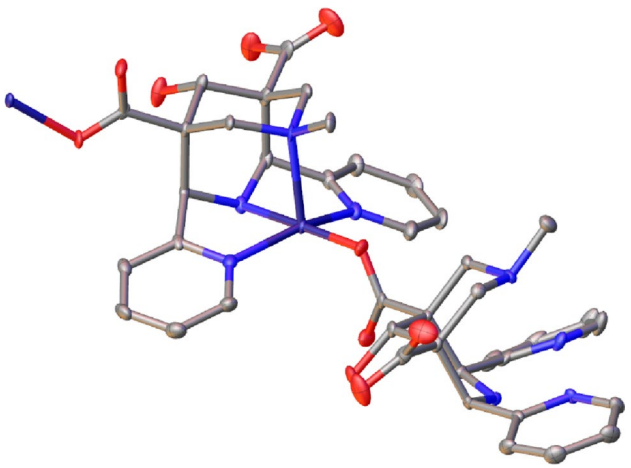

Fig. 3 Olex2 plot of the crystal structure analysis of $[(L^2)Cu^{II}(L^2)]^+$. Counterions, H-atoms and co-crystallized solvent molecules are omitted for clarity, ellipsoids are shown at 50% probability level. Color code: blue: N, red: O, dark blue: Cu, grey: C

as not all zirconium cations are freely accessible. Some may be partially blocked by water or modulators in the pores or by residual carboxylic acids that were not removed after NU-1000 synthesis or through the washing protocol [67].

To ensure that this did not result in mere surface loading, as in the immobilization of the free ligand, PXRD and ATR-FTIR measurements were performed. For this, one sample of untreated NU-1000 and three treated NU-1000 samples with different loadings of the copper complex were analyzed. Samples with calculated loadings of 0.4%, 3.8%, and 21.6% were selected. The first sample serves primarily as a control to reveal changes induced by the washing protocol, whereas the second and third samples are intended to highlight differences with increasing complex concentration. ATR-FTIR spectra were recorded for all samples. The resulting spectra are shown in Fig. 6 (full spectra are shown in the SI Figures S 27 - S 30). In the OH region, a sharp band at 3675 cm^{-1} was observed, which was assigned to μ_3-OH vibrations [68]. A pronounced difference among the spectra is observed in the C–H region. The untreated NU-1000 sample exhibits a band at 2748 cm^{-1}, attributable to the C–H vibration of formate bound to the Zr nodes, which can form during synthesis in DMF [69]. Additional C–H vibrations of the formate ligand appear between 2800 and 3000 cm^{-1} [70]. Notably, these bands are most prominent in the untreated NU-1000; however, even at a loading of only 0.4% they are no longer present or are markedly attenuated. Only for the sample with a 21.6% loading a shoulder reappears at 2861 cm^{-1}, indicating incomplete displacement of formate ligands. Changes are also evident in the carbonyl region: the peak maxima are slightly shifted relative to pristine NU-1000, and the relative signal intensities are altered.

Subsequently, PXRD patterns were recorded for the same samples (see SI Figure S 25 + S 26). The resulting lattice parameters as well as the calculated occupancy are shown

Table 1 Selected bond lengths and angles of the crystal structures of $[(L^1)Cu^{II}(X)]^{n+}$ with various counterions and $[(L^2)Cu^{II}(L^2)]^+$. Distances are given in (Å) and angles in (°)

Bond length (Å)	$[(L^1)Cu^{II}(OAc)]^{+*}$	$[(L^1)Cu^{II}(SO_4)]^*$	$[(L^1)Cu^{II}(NO_3)]^+$	$[(L^1)Cu^{II}(MeCN)]^{2+*}$	$[(L^1)Cu^{II}(Cl)]^+$[53]	$[(L^2)Cu^{II}(L^2)]^+$
Cu-N[3]	1.985(4)	1.990(5)	1.986(3)	2.272(6)	2.007(2)	1.984 (3)
Cu-N[7]	2.286(4)	2.313(5)	2.336(4)	1.964(6)	2.358(2)	2.233 (3)
Cu-py	2.048(4)/2.016(4)	2.027(5)/ 2.009(6)	2.005(3)/ 2.018(3)	2.022(6)/ 2.024(6)	2.013 (2)/ 2.009(2)	2.037 (3)/ 2.020 (3)
Cu-X	1.940(4)	1.921(4)	1.967(4)	1.991(6)	2.228 (6)	1.933 (3)
Py1-Cu-py2	3.983	3.975	3.966	3.964	4.022	4.067
N3-Cu-X angle (°)	3.919	3.907	3.944	3.943	4.235	3.917
N3-Cu-N7	83.53(15)	82.5(2)	83.03(12)	84.7(2)	81.25 (6)	85.40 (11)

* hydrolyzed at C^9 ($C{=}O \rightarrow C(OH)_2$)

Table 2 Absorption maxima and redox potentials of the various complexes in MeCN, MeOH or water. All measurements were performed under inert gas with dry solvents, except the measurement of $[(L^1)Cu^{II}(MeCN)](OTf)_2$ in MeOH and measurements in water

Complex	Λ (nm) [ε ($mol^{-1}L^{-1}$)] MeCN	Λ (nm) [ε ($mol^{-1}L^{-1}$)] MeOH	$E^{1/2}$ (mV) vs. fc/fc^+ MeCN	$E^{1/2}$ (mV) vs. fc/fc^+ MeOH
$[(L^1)Cu^{II}(MeCN)](OTf)_2$	619 [131], 913 [32] [39]	651 [95]	-394[39]	-728
$[(L^1)Cu^{II}(OAc)](OAc)$		629 [118]		-864
$[(L^1)Cu^{II}(NO_3)](NO_3)$	640 [107]	603 [103], 708 [80]		-820
$[(L^1)Cu^{II}(SO_4)]$		611 [54], 706 [51]	-484	-844
$[(L^1)Cu^{II}(MeCN)](ClO_4)_2$	620 [110] 898 [23]	600 [78], 717 [61]		-828
$[(L^1)Cu^{II}(Cl)]Cl$		617 [80], 706 [82]	-837	-862
	Λ (nm) [ε ($mol^{-1}L^{-1}$)] H_2O		**E^{pc}(mV) vs. $[Fe(CN)_6]^{3-/4-}$ H_2O**	
$[(L^2)Cu^{II}(H_2O)](OTf)_2$	590 [70] 661 [78]		-633	

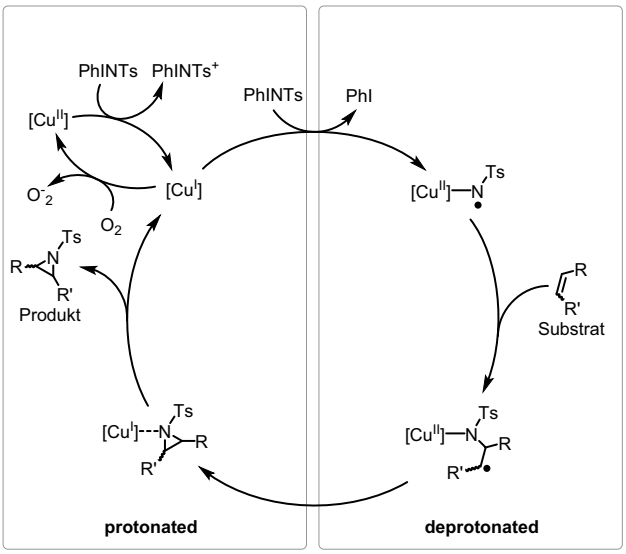

Fig. 4 Proposed reaction mechanism for $[(L^1)Cu^{II}(MeCN)]^{2+}$ [38]

Table 3 Yields and standard deviation of the various reactions in the catalytic conversion of styrene to the corresponding aziridine (cat: ox: substrate 1:20:100, 5 mM Cu(II) complex in MeCN) under ar and air

Complex	Yield (%) Ar	Yield (%) Air
$[(L^1)Cu^{II}(MeCN)](OTf)_2$	82.0 ± 1.5[39]	49.2 ± 2.6
$[(L^1)Cu^{II}(OAc)](OAc)$	58.6 ± 0.3	48.6 ± 2.1
$[(L^1)Cu^{II}(NO_3)](NO_3)$	64.2 ± 3.1	57.1 ± 2.1
$[(L^1)Cu^{II}(SO_4)]$	67.4 ± 0.4	52.9 ± 0.0
$[(L^1)Cu^{II}(MeCN)](ClO_4)_2$	68.3 ± 7.8	52.9 ± 1.1
$[(L^1)Cu^{II}(Cl)]Cl$	37.3 ± 17.3	53.4 ± 0.5
$[(L^2)Cu^{II}(MeCN)](OTf)_2$	57.1 ± 5.3	21.9 ± 10.1
Blank	0.6 ± 0.6[38]	7.4 ± 3.8

in Table 4. The measured unit-cell parameters fall within the range of literature values. Goetjen et al. reported for NU-1000, after $CrCl_2$ treatment of the Zr_6O_6 nodes (occupancy ≈ 0.25), values of a = 39.433 Å and c = 16.256 Å [71]. For bromide-functionalized nodes, values of a = 39.602 Å and c = 16.440 Å are reported [72], whereas the guest-free reference shows values of a = 39.268 Å and c = 15.567 Å [73]. The changes observed in our datasets correspond to

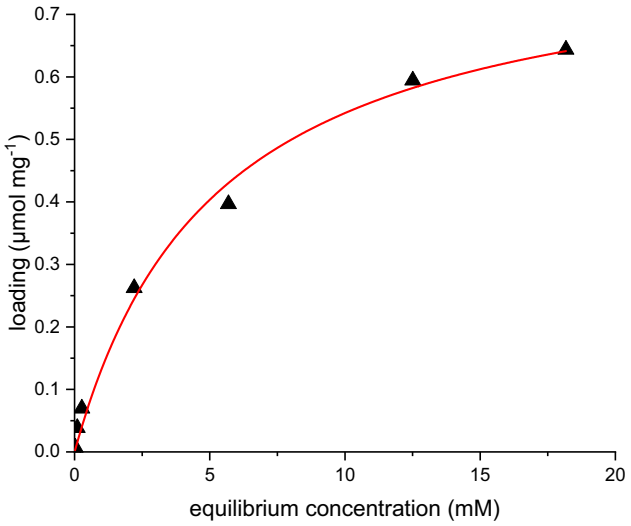

Fig. 5 Loading isotherm of $[(L^2)Cu^{II}(H_2O)]^{2+}$ on NU-1000 in water (pH 2, 65 °C, 24 h). Parameter: q_{max} = 0.82±0.04 µmol/mg and K_L = 0.19±0.03 L mmol^{-1}. (Fit: $q_{max}\frac{K_L C}{1+K_L C}$; χ^2_{red}= 4.96 • 10^{-3}; Because only a single measurement was available for each concentration level, the reported values should be interpreted with caution.)

a moderate adjustment of the unit-cell parameters, with no symmetry breaking or significant peak splitting. However, the occupancy calculated from the lattice parameters shows a trend opposite to expectations. According to these parameters, the untreated NU-1000 sample shows the highest pore occupancy; it gradually decreases with increasing copper content derived from the UV/vis loadings. This correlates with the literature data on cell parameter a, which decreases with pore loading (e.g., Br^- functionalization) [9]. Additionally, performed Rietveld/Le Bail refinements with different starting models indicate that the additional copper ion is consistently located in the mesopores; models placing copper ions in the micropores are not computationally stable and yield poorer fits.

Although the occupancy derived from the PXRD data evaluation and the loading calculated from the UV/vis data initially appear contradictory, a consistent picture emerges. The sample whose UV/vis evaluation yields a loading of 21.6% shows a very low pore occupancy in PXRD; at the same time, it is the only copper-treated sample in which shoulders of the C–H vibrations remain visible in the ATR-FTIR spectra, assignable to formate bound to the Zr_6O_6 nodes. By contrast, these bands are markedly weaker or absent in the lower-loaded samples, while the PXRD occupancy is higher. Supported by (i) loading isotherms of the sole ligand, (ii) SEM images showing crosslinking of NU-1000 crystals via ligand crosslinking, and (iii) crystal structures that confirm the ligand's propensity to crosslink, we infer that at high complex concentration in the incubation solution a near-surface crosslinking occurs. As a result, pore openings are partially blocked, exchange within the MOF interior is hindered, formate cannot be displaced from the nodes, and the pore occupancy in PXRD remains low - while a high overall loading is achieved at the MOF surface. Conversely, samples incubated at lower complex concentration are not subject to pronounced crosslinking. Here, guest species such as formate can be removed by treatment with aqueous HCl and complex. Accordingly, the ATR-FTIR formate bands disappear, and the PXRD occupancy increases because more species can access the pores of the MOF. These results thus reveal a concentration-dependent transition from predominantly intraparticle immobilization at low complex concentrations to near-surface crosslinking and impaired mass transport at high concentrations. Both are unfavorable for catalysis. In the following, immobilized samples with high surface loading are examined for their stability, since they may still provide many directly accessible active centers despite the loss of intraporous area. The aim is to establish whether such surface loading remains stable under reaction conditions. Immobilisates with low copper loading will not be investigated further. Although PXRD analysis suggests a high loading, the loading determined by UV/vis is very low, and since only low concentrations of the copper complex were used, the number of active center's is insufficient. The apparently high loading in PXRD is likely attributable to other guest molecules that were not completely removed.

Stability of immobilisates

Although characterization of the immobilisate indicated predominantly surface binding, we nevertheless performed stability tests. To assess the stability of immobilized $[(L^2)Cu^{II}(H_2O)]^{2+}$ during the aziridination reaction in MeCN, two NU-1000 immobilized sample were weighed in (direct immobilization, 65 °C, loading q = 0.64 µmol/mg and 0.59 µmol/mg), treated with 1.000 mL acetonitrile, and incubated at T = 25 °C for 24 h in a thermoshaker (see SI for detailed work instructions and visualization of data, Figure S 21). The copper concentration in the supernatant was then determined by ICP-OES. Four washing cycles were performed for the immobilisates. In both samples, copper leaching was detected and persisted through the fourth cycle, with residual concentrations of approximately 1.5 ng/mL. In total, more than 15% of the copper was leached over the four washing cycles. Due to the ongoing leaching of copper species, reliable catalysis experiments with the immobilisates were not possible: the contribution of the homogeneous reaction cannot be separated from the intrinsic activity of the immobilisates. In addition, potential metal contamination rules out certain fields of application. For these reasons,

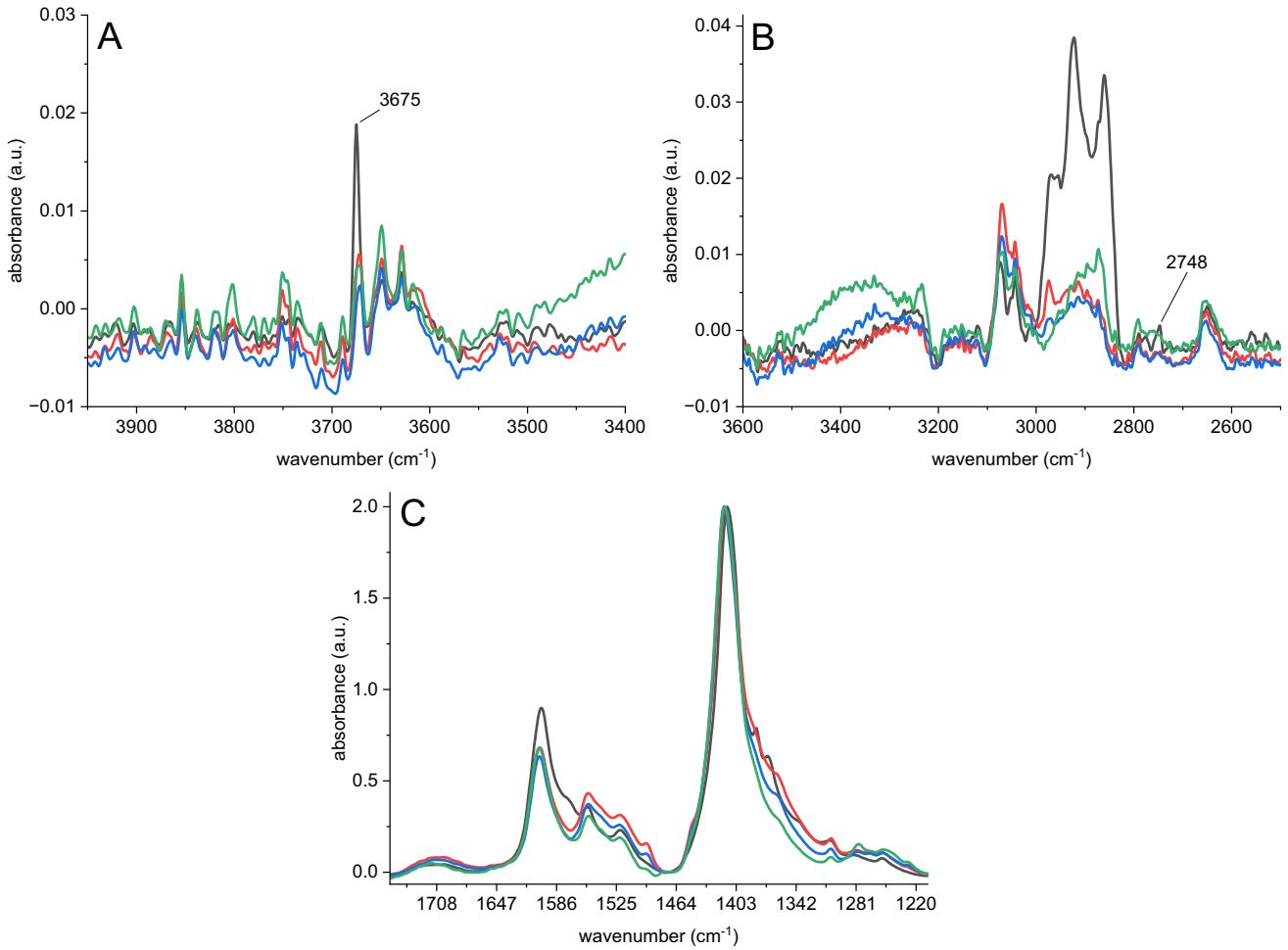

Fig. 6 ATR-FTIR spectra of untreated NU-1000 (black) and loaded samples with 0.4% (0.007 µmol/mg, red); 3.8% (0.070 µmol/mg, blue); and 21.6% (0.397 µmol/mg, green). Shown are different spectral sections: A: O–H region (3675 cm^{-1} ν (μ_3-OH)); B: C–H region (2748 cm^{-1}, ν (C-$H_{formate}$)); C: carbonyl vibrations. Spectra were normalized to the band at 1412 cm^{-1}. For panels A and B, a baseline correction was applied by setting the absorbance at 4494 cm^{-1} to zero

Table 4 Loadings determined from UV/vis measurements, together with the lattice parameters a and c, and the corresponding occupancy calculated from PXRD measurements

Sample	Loading (µmol/mg)	Loading (%)	a (Å)	c (Å)	Occupancy PXRD
NU-1000	0	0	39.627 (0.011)	16.593 (0.006)	0.39
1	0.007	0.4	39.576 (0.015)	16.527 (0.006)	0.21
2	0.07	3.8	39.503 (0.031)	16.457 (0.013)	0.1
3	0.397	21.6	39.430 (0.010)	16.622 (0.005)	0.08

we did not perform heterogeneous catalysis experiments with the prepared immobilisates.

Conclusion

In this work, we have synthesized and characterized a copper-bispidine complex bearing carboxylic acid groups on the backbone. Owing to its structural features, this complex is highly prone to crosslinking and the formation of one-dimensional aggregates. Like many bispidine-based copper complexes, it exhibits catalytic activity in the aziridination of styrene. By varying the counterions of the copper complex, we showed that under an inert atmosphere the nature of the counterion has a pronounced effect on the catalytic yield. Under air, the outcome is largely governed by oxidation of the active Cu(I) species and the formation of aqua/hydroxido complexes, which reduces the impact of the counterion. Attempts to immobilize the complex on NU-1000 revealed that, particularly at high complex concentrations, immobilization remains largely confined to the external surface and is accompanied by substantial crosslinking and significant

copper leaching. As a consequence, reliable heterogeneous catalytic tests of the resulting materials could not be carried out. Although the present results highlight the limitations of the current immobilization strategy, they provide promising starting points for future work. Instead of transforming the methyl esters on the bispidine backbone, a specific functional group could be introduced for covalent anchoring, e.g., at N^7, to avoid surface crosslinking and achieve more reliable intrapore coverage. In addition, changing the carrier material offers new perspectives: Beads made of suitable polymers or inorganic materials that allow stable covalent anchoring are a promising alternative to MOFs, minimizing leaching and increasing industrial applicability.

Supplementary Information The online version contains supplementary material available at https://doi.org/10.1007/s10847-026-01334-3.

Acknowledgements K.B. gratefully acknowledges financial support from the KIT Center 'Materials in Technical and Life Sciences' (MaTeLiS). The authors thank Matthias Franzreb and Peter Comba for the access to their laboratories. Furthermore, the authors thank Marita Heinle and Ulrich Thiele from KIT for performing the ICP-OES analyses and SEM measurements. Furthermore, the authors would like to thank Juliane Diehm for the fruitful discussions.

Author contributions The first draft of the manuscript was written by K.B. and all authors commented on previous versions of the manuscript. All authors read and approved the final manuscript. Conceptualization (K.B.), Investigation (T.K., N.S., T.S., F.K., P.G.W., S.H., T.J., K.B.), Resources (K.B.), Supervision (K.B.)

Funding Open Access funding enabled and organized by Projekt DEAL.

Data availability Crystallographic data for the structures reported in this article have been deposited at the Cambridge Crystallographic Data Centre, under deposition numbers 2513653, 2513655, 2513652, 2513654, 2513651 and 2513650. Copies of the data can be obtained free of charge via https://www.ccdc.cam.ac.uk/structures/. All other relevant data generated and analysed during this study, which include experimental, spectroscopic and crystallographic data, are included in this article and its supplementary information.

Declarations

Competing interests The authors declare no competing interests.

References

1. Bailey, D.C., Langer, S.H.: Immobilized Transition-Metal carbonyls and related catalysts. Chem. Rev. **81**(2), 109–148 (1981).
2. Rakhtshah, J.: A comprehensive review on the synthesis, characterization, and catalytic application of transition-metal Schiff-base complexes immobilized on magnetic Fe3O4 nanoparticles. Coord. Chem. Rev. **467**, 214614 (2022). https://doi.org/10.1016/j.ccr.2022.214614
3. Benaglia, M., Puglisi, A. (eds.): Catalyst immobilization: methods and applications. Wiley (2020)
4. Corma, A.: Attempts to fill the gap between enzymatic, homogeneous, and heterogeneous catalysis. Catal. Rev. - Sci. Eng. **46**, 369–417 (2004). https://doi.org/10.1081/CR-200036732
5. Sun, Q., Wang, N., Yu, J.: Advances in catalytic applications of Zeolite-Supported metal catalysts. Adv. Mater. **33**, 1–37 (2021). https://doi.org/10.1002/adma.202104442
6. Shinde, P.S., Suryawanshi, P.S., Patil, K.K., Belekar, V.M., Sankpal, S.A., Delekar, S.D., Jadhav, S.A.: A brief overview of recent progress in porous silica as catalyst supports. J. Compos. Sci. **5**, 1–17 (2021). https://doi.org/10.3390/jcs5030075
7. Liu, J., Goetjen, T.A., Wang, Q., Knapp, J.G., Wasson, M.C., Yang, Y., Syed, Z.H., Delferro, M., Notestein, J.M., Farha, O.K., Hupp, J.T.: MOF-enabled confinement and related effects for chemical catalyst presentation and utilization. Chem. Soc. Rev. **51**, 1045–1097 (2022). https://doi.org/10.1039/d1cs00968k
8. Shiri, P., Aboonajmi, J.: A systematic review on silica-, carbon-, and magnetic materials-supported copper species as efficient heterogeneous nanocatalysts in click reactions. Beilstein J. Org. Chem. **16**, 551–586 (2020). https://doi.org/10.3762/bjoc.16.52
9. Mercuri, G., Moroni, M., Galli, S., Tuci, G., Giambastiani, G., Yan, T., Liu, D., Rossin, A.: Temperature-Dependent nitrous Oxide/Carbon dioxide Preferential adsorption in a Thiazolium-Functionalized NU-1000 Metal–Organic framework. ACS Appl. Mater. Interfaces. **13**, 58982–58993 (2021). https://doi.org/10.1021/acsami.1c21437
10. Lyu, X., Gonzalez, R., Horton, A., Li, T.: Immobilization of enzymes by polymeric materials. Catalysts. **11**, 1211 (2021)
11. Goetjen, T.A., Knapp, J.G., Syed, Z.H., Hackler, R.A., Zhang, X., Delferro, M., Hupp, J.T., Farha, O.K.: Ethylene polymerization with a crystallographically well-defined metal–organic framework supported catalyst. Catal. Sci. Technol. **12**, 1619–1627 (2022). https://doi.org/10.1039/d1cy01990b
12. Yang, Y., Zhang, X., Kanchanakungwankul, S., Lu, Z., Noh, H., Syed, Z.H., Farha, O.K., Truhlar, D.G., Hupp, J.T.: Unexpected spontaneous evolution of Catalytic, MOF-Supported single Cu(II) cations to Catalytic, MOF-Supported Cu(0) nanoparticles. J. Am. Chem. Soc. **142**, 21169–21177 (2020). https://doi.org/10.1021/jacs.0c10367
13. Pan, Y., Sanati, S., Nadafan, M., Abazari, R., Gao, J., Kirillov, A.M.: Postsynthetic modification of NU-1000 for designing a Polyoxometalate-Containing nanocomposite with enhanced Third- order nonlinear optical performance. Inorg. Chem. **61**, 18873–18882 (2022). https://doi.org/10.1021/acs.inorgchem.2c02709
14. Gorla, S., Mariana, L.D., Abeynayake, N.S., Kaphan, D.M., Williams, D.R., Martis, V., Lara-garc, H.A., Donnadieu, B., Lopez, N., Ibarra, I.A., Montiel-palma, V.: Functionalized NU-1000 with an iridium organometallic fragment: SO2 capture enhancement. ACS Appl. Mater. Interfaces. **12**, 41758–41764 (2020). https://doi.org/10.1021/acsami.0c11615

15. Greifenstein, R., Ballweg, T., Hashem, T., Gottwald, E., Achauer, D., Kirschhöfer, F., Nusser, M., Brenner-Weiß, G., Sedghamiz, E., Wenzel, W., Mittmann, E.: MOF-Hosted Enzymes for Continuous Flow Catalysis in Aqueous and Organic Solvents. Angew. Chem. Int. Ed. **61**(18), e202117144 (2022) https://doi.org/10.1002/anie.202117144
16. Ye, N., Kou, X., Shen, J., Huang, S., Chen, G.: Metal-Organic frameworks: A new platform for enzyme immobilization. CHemBioCHem. **21**, 2585–2590 (2020). https://doi.org/10.1002/cbic.202000095
17. Dhakshinamoorthy, A., Asiri, A.M., Garcia, H.: Formation of C-C and C-Heteroatom bonds by C-H activation by metal organic frameworks as catalysts or supports. ACS Catal. **9**, 1081–1102 (2019). https://doi.org/10.1021/acscatal.8b04506
18. López-Magano, A., Mas-Ballesté, R., Alemán, J.: Predesigned covalent organic frameworks as effective platforms for Pd(II) coordination enabling Cross-Coupling reactions under sustainable conditions. Adv. Sustain. Syst. **6**(3), p2100409 (2022) https://doi.org/10.1002/adsu.202100409
19. Lawrence, A.S., Martin, N., Sivakumar, B., Cirujano, F.G., Dhakshinamoorthy, A.: Palladium-based metal organic frameworks as heterogeneous catalysts for C– C couplings. ChemCatChem. **14**(18), e202200403 (2022) https://doi.org/10.1002/cctc.202200403
20. Pareras, G., Tiana, D., Poater, A.: MOF encapsulation of Ru olefin metathesis catalysts to block catalyst decomposition. Catalysts. **10**(6), 687 (2020) https://doi.org/10.3390/catal10060687
21. Roesky, P.W., Bhunia, A., Lan, Y., Powell, K., Kureti, S.: Salen-based metal – organic frameworks of nickel and the lanthanides. Chem. Commun. **47**, 2035–2037 (2011). https://doi.org/10.1039/c0cc04881j
22. Hübner, S., De Vries, J.G., Farina, V.: Why does industry not use immobilized transition metal complexes as catalysts? Adv. Synth. Catal. **358**, 3–25 (2016). https://doi.org/10.1002/adsc.201500846
23. Cantillo, D., Kappe, C.O.: Immobilized transition metals as catalysts for cross-couplings in continuous flow - A critical assessment of the reaction mechanism and metal leaching. ChemCatChem. **6**, 3286–3305 (2015). https://doi.org/10.1002/cctc.201402483
24. Koosha, S., Ghorbani-Vaghei, R., Alavinia, S.: Copper-anchored polysulfonamide-modified UiO- 66-NH2/sodium alginate nanocatalyst for sustainable synthesis of 1,2,3-triazoles. Nanoscale Adv. **7**, 1937–1945 (2025). https://doi.org/10.1039/d4na01055h
25. Singh, R., Singh, G., George, N., Singh, G., Gupta, S., Singh, H., Kaur, G., Singh, J.: Copper-based metal–organic frameworks (MOFs) as an emerging catalytic framework for click chemistry. Catalysts. **13**(1), 130 (2023) https://doi.org/10.3390/catal13010130
26. Luz, I., Llabrés, I., Xamena, F.X., Corma, A.: Bridging homogeneous and heterogeneous catalysis with mofs: Click reactions with Cu-MOF catalysts. J. Catal. **276**, 134–140 (2010). https://doi.org/10.1016/j.jcat.2010.09.010
27. Deria, P., Bury, W., Hod, I., Kung, C., Karagiaridi, O., Hupp, J.T., Farha, O.K.: MOF functionalization via Solvent-Assisted ligand incorporation: Phosphonates vs carboxylates. Inorg. Chem. **54**, 2185–2192 (2015). https://doi.org/10.1021/ic502639v
28. Deria, P., Mondloch, J.E., Tylianakis, E., Ghosh, P., Bury, W., Snurr, R.Q., Hupp, J.T., Farha, O.K.: Perfluoroalkane functionalization of NU-1000 via Solvent-Assisted ligand incorporation: Synthesis and CO 2 adsorption studies. J. Am. Chem. Soc. **14**, 20–23 (2013)
29. Deria, P., Bury, W., Hupp, J.T., Farha, O.K.: Versatile functionalization of the NU-1000 platform by solvent-assisted ligand incorporation. Chem. Commun. **50**, 1965–1968 (2014). https://doi.org/10.1039/c3cc48562e
30. Rogge, S.M., Bavykina, A., Hajek, J., Garcia, H., ASepu´lveda-Escribano, A.I.O.-S., Vimont, A., Clet, A., Bazin, G., Kapteijn, P., Daturi, F., Ramos-Fernandez, M., Xamena, E.V.L., Van Speybroeck, F.X., Gascon, V.: J.: Metal–organic and covalent organic frameworks as single-site catalysts. Chem Soc Rev. 46(11), pp.3134-3184 (2017) https://doi.org/10.1039/c7cs00033b
31. Tu, W., Xu, Y., Yin, S., Xu, R.: Rational design of catalytic centers in crystalline frameworks. Adv. Mater. **30**, 1707582 (2018). https://doi.org/10.1002/adma.201707582
32. Zhang, K., Goswami, S., Noh, H., Lu, Z., Sheridan, T., Duan, J., Dong, W., Hupp, J.T.: An iron-porphyrin grafted metal – organic framework as a heterogeneous catalyst for the photochemical reduction of CO 2. J. Photochem. Photobiol. **10**, 100111 (2022). https://doi.org/10.1016/j.jpap.2022.100111
33. Nakagaki, S., Mantovani, K.M., Machado, G.S., De Freitas Castro, K.A.D., Wypych, F.: Recent advances in solid catalysts obtained by metalloporphyrins immobilization on layered anionic exchangers: A short review and some new catalytic results. Molecules. **21**, 290–315 (2016). https://doi.org/10.3390/molecules21030291
34. Feng, L., Wang, K.Y., Joseph, E., Zhou, H.C.: Catalytic porphyrin framework compounds. Trends Chem. **2**, 555–568 (2020). https://doi.org/10.1016/j.trechm.2020.01.003
35. Bleher, K., Cieslik, P., Comba, P.: Bispidine coordination chemistry. Dalt Trans. **54**, 4405 (2025)
36. Lippi, M., Murelli, A., Rossi, P., Paoli, P., Cametti, M.: Different topologies of Hg(II)-Bispidine 1D coordination polymers: Dynamic behaviour in solvent adsorption and exchange processes. Chem. – Eur. J. **28**, e202200420 (2022). https://doi.org/10.1002/chem.202200420
37. Cametti, M.: 1D coordination polymers as promising adsorbers for volatile organic pollutants: The case of Bispidine based materials. Coord. Chem. Rev. **549**, 217261 (2026). https://doi.org/10.1016/j.ccr.2025.217261
38. Josephy, T., Heiduk, M., Saxl, T., Bleher, K.: Reversible deprotonation as crucial step in Bispidine copper-catalyzed aziridination reaction. Inorganica Chim. Acta. **579**, 122587 (2025). https://doi.org/10.1016/j.ica.2025.122587
39. Bleher, K., Comba, P., Gast, M., Kronenberger, S., Josephy, T.: Copper-bispidine-catalyzed aziridination – A new twist in small molecule activation. Inorganica Chim. Acta. **532**, 120752 (2022). https://doi.org/10.1016/j.ica.2021.120752
40. Martos, M., Pastor, I.M.: Node Modification of Metal-Organic Frameworks for Catalytic Applications. ChemistryOpen. **14**(7), e202400428 (2025). https://doi.org/10.1002/open.202400428
41. Kung, C., Otake, K., Drout, R.J., Goswami, S., Farha, O.K., Hupp, J.T.: Post-Synthetic Cyano-ferrate(II) functionalization of a Metal–Organic Framework, NU-1000. Langmuir. **39**, 4936–4942 (2023). https://doi.org/10.1021/acs.langmuir.2c03354
42. Islamoglu, T., Otake, K.I., Li, P., Buru, C.T., Peters, A.W., Akpinar, I., Garibay, S.J., Farha, O.K.: Revisiting the structural homogeneity of NU-1000, a Zr-based metal-organic framework. CrystEngComm. **20**, 5913–5918 (2018). https://doi.org/10.1039/c8ce00455b
43. Abazari, R., Sanati, S., Bajaber, M.A., Javed, M.S., Junk, P.C., Nanjundan, A.K., Qian, J., Dubal, D.P.: Design and advanced manufacturing of NU-1000 Metal–Organic frameworks with future perspectives for environmental and renewable energy applications. Small. **20**, 1–44 (2024). https://doi.org/10.1002/smll.202306353
44. Comba, P., Grimm, L., Orvig, C., Rück, K., Wadepohl, H.: Synthesis and coordination chemistry of hexadentate Picolinic acid based Bispidine ligands. Inorg. Chem. **55**, 12531–12543 (2016). https://doi.org/10.1021/acs.inorgchem.6b01787
45. Samhammer, A., Holzgrabe, U., Haller, R.: Synthese, stereochemie und analgetische wirkung von 3,7-Diazabicyclo[3.3.1]nonan-9-onen und 1,3-Diazaadamantan-6-onen1). Arch. Pharm.

(Weinheim). **322**, 551–555 (1989). https://doi.org/10.1002/ardp.19893220908
46. Evans, D.A., Faul, M.M., Bilodeau, M.T.: Copper-Catalyzed aziridination of olefins by (N-(p-Toluenesulfonyl)imino)phenyliodinane. J. Org. Chem. **56**, 6744–6746 (1991)
47. Evans, D.A., Paul, M.M., Bilodeau, M.T., Faul, M.M., Bilodeau, M.T.: Development of the Copper-Catalyzed olefin aziridination reaction. J. Am. Chem. Soc. **116**, 2742–2753 (1994)
48. Yamada, Y., Yamamoto, T., Okawara, M.: Synthesis and reaction of new type I–N ylide, n-Tosyliminoiodinane. Chem. Lett. **4**(4), 361–362 (1975)
49. Dolomanov, O.V., Bourhis, L.J., Gildea, R.J., Howard, J.A.K., Puschmann, H.: OLEX2: A complete structure solution, refinement and analysis program. J. Appl. Crystallogr. **42**, 339–341 (2009). https://doi.org/10.1107/S0021889808042726
50. Pawley, G.S.: Unit-cell refinement from powder diffraction scans. Appl. Crystallogr. **14**, 357–361 (1981)
51. Bruker AXS, TOPAS V6: General profile andstructure analysis software for powder diffraction data. – Users Manual, Bruker-AXS, Karlsruhe, Germany (2017)
52. Gullick, J., Ryan, D., Mcmorn, P., Bethell, D., King, F., Hancock, F., Hutchings, G., Catalysts, J.M.: Catalytic asymmetric heterogeneous aziridination of styrene using Cu 2+ -exchanged zeolite Y: Effect of the counter-cation on enantioselectivity and on the reaction profile. New. J. Chem. **28**, 1470–1478 (2004)
53. Schneider, C.: Synthese und Charakterisierung neuer BispidinLiganden und ihrer Metallkomplexe für die potentielle Anwendung in der Nuklearmedizin. Masterarbeit, Ruprecht-Karls-Universität Heidelberg. (2015)
54. Born, K., Comba, P., Ferrari, R., Lawrance, G.A., Wadepohl, H.: Stability constants: A new twist in transition metal Bispidine chemistry. Inorg. Chem. **46**, 458–464 (2007). https://doi.org/10.1021/ic061501+
55. Born, K., Comba, P., Kerscher, M., Linti, G., Pritzkow, H., Rohwer, H.: Distortional isomerism with Copper (I) complexes of 3, 7-diazabicyclo [3.3. 1] nonane derivatives. Dalton Trans. (2):362–367. (2009) https://doi.org/10.1039/b810833a
56. Belford, R.L., Calvin, M., Belford, G.: Bonding in copper (II) chelates: Solvent effects in their visible absorption spectra. J. Chem. Phys. **26**(5), 1165–1174 (1957)
57. Comba, P., Haaf, C., Helmle, S., Karlin, K.D., Pan□dian, S., Waleska, A.: Dioxygen reactivity of new bispidine-copper complexes Peter. Inorg. Chem. **51**, 2841–2851 (2012). https://doi.org/10.1021/ic2019296.Dioxygen
58. Comba, P., Lang, C., De Laorden, C.L., Muruganantham, A., Rajaraman, G., Wadepohl, H., Zajaczkowski, M.: The mechanism of the (bispidine)copper(ii)-catalyzed aziridination of styrene: A combined experimental and theoretical study. Chem. - Eur. J. **14**, 5313–5328 (2008). https://doi.org/10.1002/chem.200701910
59. Brandt, P., Södergren, M.J., Andersson, P.G., Norrby, P.O.: Mechanistic studies of copper-catalyzed alkene aziridination. J. Am. Chem. Soc. **122**, 8013–8020 (2000). https://doi.org/10.1021/ja993246g
60. Rodríguez, M.R., Rodríguez, M., López-Resano, A., Pericàs, S., Díaz-Requejo, M.A., Maseras, M.M., Pérez, F.: Non-innocent role of the halide ligand in the Copper-Catalyzed olefin aziridination reaction. ACS Catal. **13**, 706–713 (2023). https://doi.org/10.1021/acscatal.2c05069
61. Mohr, F., Binfield, S.A., Fettinger, J.C., Vedernikov, A.N.: A Practical, Fast, and High-Yielding aziridination procedure using simple Cu (II) complexes containing N-Donor Pyridine-Based ligands. J. Org. Chem. **70**, 4833–4839 (2005)
62. Li, Y., He, J., Khankhoje, V., Herdtweck, E., Köhler, K., Stocheva, O., Cokoja, M., Kühn, F.E.: Copper(II) complexes incorporating poly/perfluorinated alkoxyaluminate-type weakly coordinating anions: Syntheses, characterization and catalytic application in stereoselective olefin aziridination. Dalt Trans. **40**, 5746–5754 (2011). https://doi.org/10.1039/c1dt10280j
63. Rach, S.F., Kühn, F.E.: Nitrile ligated transition metal complexes with weakly coordinating counteranions and their catalytic applications. Chem. Rev. **109**, 2061–2080 (2009)
64. Company, A., Go, L., Korendovych, I.V., Ribas, X.: Fast O 2 binding at dicopper complexes containing Schiff-Base dinucleating ligands. Inorg. Chem. **46**, 4997–5012 (2007)
65. Li, Y., Diebl, B., Raith, A., Kühn, F.E.: Syntheses of acetonitrile ligated copper complexes with perfluoroalkoxy aluminate as counter anion and their catalytic application for olefin aziridination. **49**(41), 5954–5956 (2008) https://doi.org/10.1016/j.tetlet.2008.07.162
66. Liu, J., Li, Z., Zhang, X., Otake, K., Zhang, L., Peters, A.W., Young, M.J., Bedford, N.M., Letourneau, S.P., Mandia, D.J., Elam, W., Farha, O.K., Hupp, J.T.: Introducing nonstructural ligands to Zirconia-like Metal–Organic framework nodes to tune the activity of Node-Supported nickel catalysts for ethylene hydrogenation. ACS Catal. **9**, 3198–3207 (2019). https://doi.org/10.1021/acscatal.8b04828
67. Wang, T.C., Vermeulen, N.A., Kim, I.S., Martinson, A.B.F., Stoddart, J.F., Hupp, J.T., Farha, O.K.: Scalable synthesis and post-modification of a mesoporous metal-organic framework called NU-1000. Nat. Protoc. **11**, 149–162 (2016). https://doi.org/10.1038/nprot.2016.001
68. Planas, N., Mondloch, J.E., Tussupbayev, S., Borycz, J., Gagliardi, L., Hupp, J.T., Farha, O.K., Cramer, C.J.: Defining the proton topology of the Zr6 – Based Metal–Organic framework NU-1000. J. Phys. Chem. Lett. **5**, 3716–3723 (2014)
69. Yang, D., Ortun, M.A., Bernales, V., Cramer, C.J., Gagliardi, L., Gates, B.C.: Structure and dynamics of Zr6O8 Metal–Organic framework node surfaces probed with ethanol dehydration as a catalytic test reaction. J. Am. Chem. Soc. **140**, 3751–3759 (2018). https://doi.org/10.1021/jacs.7b13330
70. Hadjiivanov, K.I., Panayotov, D.A., Mihaylov, M.Y., Ivanova, E.Z., Chakarova, K.K., Andonova, S.M., Drenchev, N.L.: Power of infrared and Raman spectroscopies to characterize Metal-organic frameworks and investigate their interaction with guest molecules. Chem. Rev. **121**, 1286–1424 (2021). https://doi.org/10.1021/acs.chemrev.0c00487
71. Goetjen, T.A., Knapp, J.G., Syed, Z.H., Hackler, R.A., Zhang, X., Delferro, M., Hupp, J.T., Farha, O.K.: Ethylene polymerization with a crystallographically well-defined metal–organic framework supported catalyst. Catal. Sci. Technol. **12**(5), 1619–1627 (2022)
72. Mercuri, G., Moroni, M., Galli, S., Tuci, G., Giambastiani, G., Yan, T., Liu, D., Rossin, A.: Temperature-Dependent Nitrous Oxide/Carbon Dioxide Preferential Adsorption in a Thiazolium-Functionalized NU-1000 Metal-Organic Framework. ACS Appl. Mater. Interfaces. **13**(49), 58982–58993 (2021). https://doi.org/10.1021/acsami.1c21437
73. Islamoglu, T., Otake, K.I., Li, P., Buru, C.T., Peters, A.W., Akpinar, I., Garibay, S.J., Farha, O.K.: Revisiting the structural homogeneity of NU-1000, a Zr-based metal–organic framework. CrystEngComm. **20**(39), 5913–5918 (2018)